Supporting Information for Quantitative reaction monitoring using parahydrogen-enhanced benchtop NMR spectroscopy

Table of Contents

SI1: Automated Data Processing

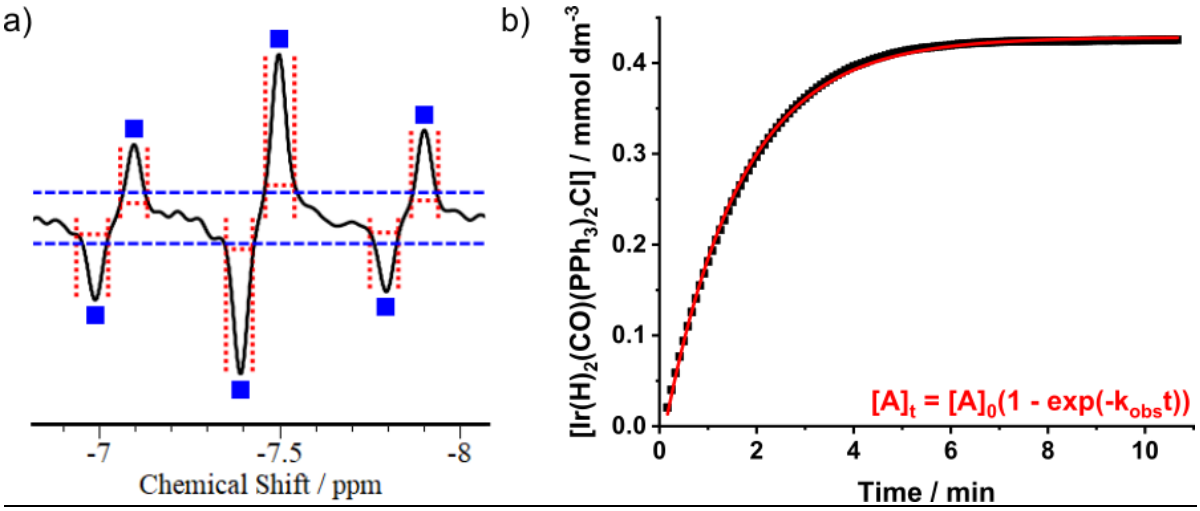

Figure S1 (a) Example output of the automatic processing macro, highlighting peak picking (blue dashed lines), integration (red dotted lines) and peak grouping (blue squares) subroutines. (b) Example product formation curve with monoexponential recovery fitting.

Automated data processing is performed within Prospa (v3.39, Magritek Ltd, Germany), with the user specifying the path for the experimental folder containing the pseudo-2D dataset. Within the data processing macro, there is an initial parameter loop and then a larger analysis loop. The initial loop is a quick analysis of a single 1D spectrum of the pseudo-2D dataset allowing for the correct parameters to be determined before doing the full analysis. After providing the location of the raw data to the macro, the parameter loop extracts the second spectrum in the pseudo-2D dataset and phases it. A peak-picking subroutine is then performed that selects for peaks if they are greater than a threshold signal value (set by the user). As the spectrum contains anti-phase hydride signals, the threshold sweep is performed using a positive and negative threshold (shown as the blue dashed

lines in Figure S1a). From the peak list, only peaks that could potentially be hydride peaks (those below 0 ppm) are stored. To remove erroneous peaks, this peak list is compared to a list of peaks to ignore (provided by the user) to ensure only the hydrides of interest are processed. Once all peaks are identified, an integration subroutine is used to generate integration regions for each peak (shown as red dashed lines in Figure S1a). At this point an optional grouping script can be performed that allows for peaks to be grouped into discrete sets (highlighted in Figure S1a as the blue squares above each peak) – this allows for spectra containing hydrides from multiple species to be differentiated and analysed individually. From this initial loop, a table of peak chemical shifts and integration regions is output to the command line for the user to check prior to full analysis. Upon full analysis, all previous steps are performed but then the integration windows are applied across the pseudo-2D dataset to acquire the integral changes for each hydride peak. Once acquired, the integrals are converted into a concentration over time for the system with all values saved into an output csv file. This csv file can then be plotted and fit to a mono-exponential recovery function to determine k_{obs} (Figure S1b).

SI2: Benchtop OPSY Experiments

The modified reaction monitoring pulse sequence to include an OPSY filter within the acquisition window is given in Figure S2. This filter acts to remove the presence of magnetisation originating from thermally-polarised species within the sample. A summary of the k_2 rate constants obtained when using either the pulse + acquire (PA) or OPSY version of the reaction monitoring pulse sequence is given in Table S1 for both high-field and low-field NMR.

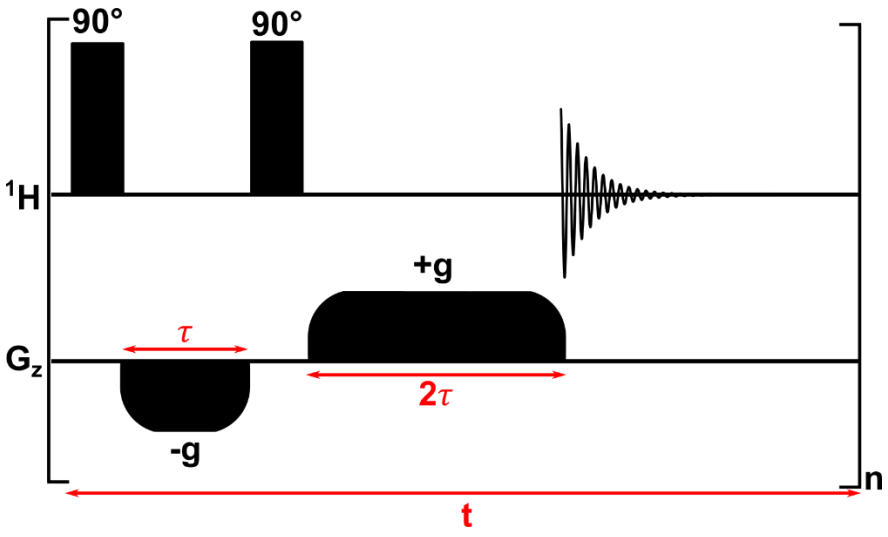

Figure S2 OPSY Reaction Monitoring pulse sequence using an OPSYd-1/2 filter.

Table S1 Summary of averaged k_2 rate constants for both PA and OPSY variants of the reaction monitoring procedure recorded at both high-field (9.4 T, 400 MHz) and low-field (1.0 T, 43 MHz).

Pulse Sequence	High-field NMR k_2 / $dm^3\ mol^{-1}\ s^{-1}$	Low-field NMR k_2 / $dm^3\ mol^{-1}\ s^{-1}$
Pulse + Acquire (PA)	(0.963 ± 0.013)	(0.792 ± 0.008)
OPSY	(0.84 ± 0.03)	(0.913 ± 0.018)

The discrepancy between the values recorded using high-field NMR were attributed to the presence of a growing background signal of residual non-hyperpolarised magnetisation in the PA experiment (highlighted in Figure S3b). The discrepancy between the values recorded using low-field NMR could not be attributed to the same feature (due to the lack of background thermal signal as highlighted Figure S4b.) In this case, the difference in value is due to the poor SNR of the OPSY spectra with a 70% drop in SNR observed between the first usable spectrum of the PA and OPSY based experiments. This poor SNR resulted in the PHIP activity being obscured by spectral noise and as such a faster than expected rate constant was obtained.

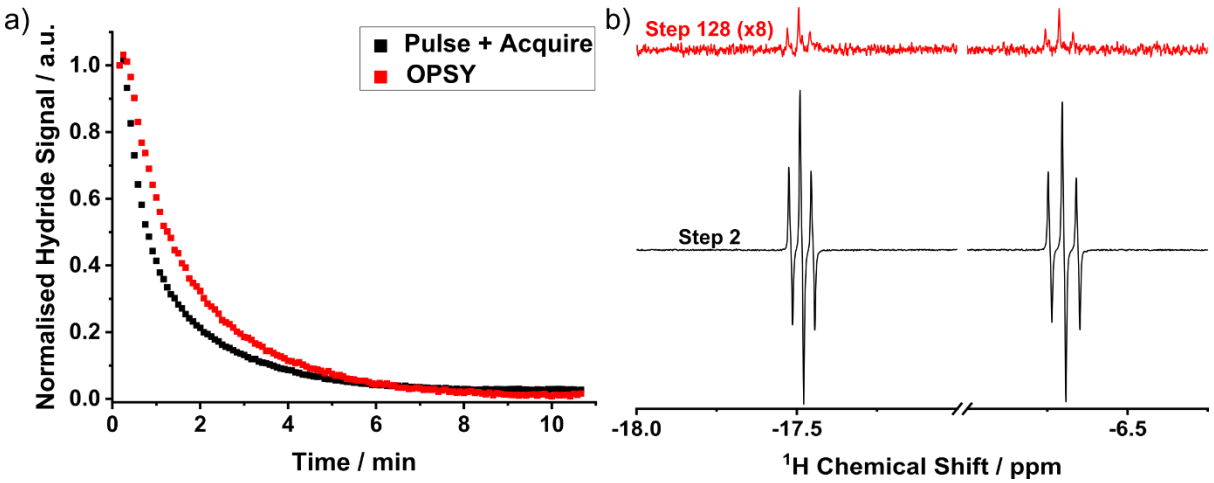

Figure S3 (a) Comparison between the PHIP activity decay curve at 9.4 T (400 MHz) when using the PA or OPSY pulse sequence to monitor pH_2 addition to Vaska's complex (0.43 mM). (b) Comparison between the first usable spectrum (black) and final spectrum (red) when using the PA pulse sequence.

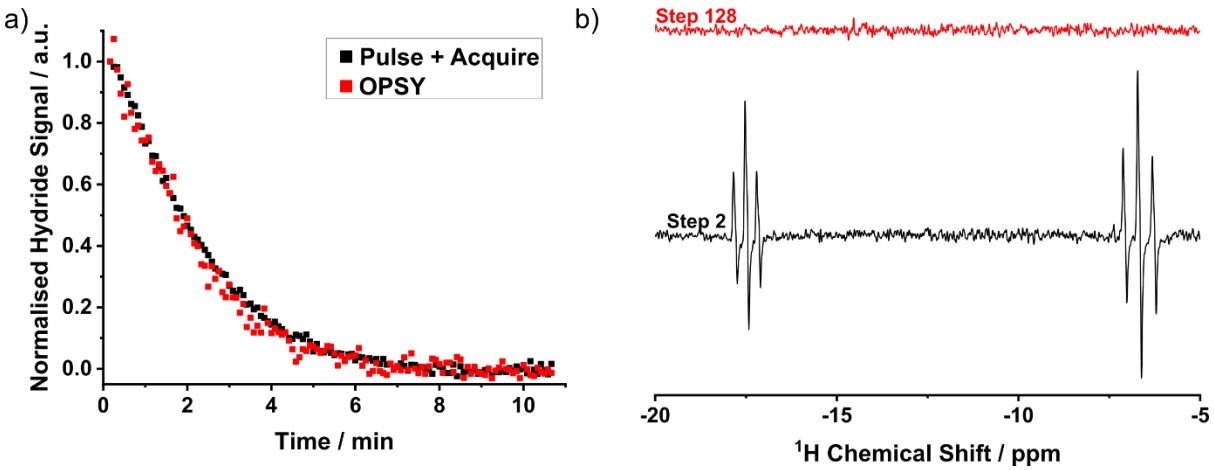

Figure S4 (a) Comparison between the PHIP activity decay curve at 1.0 T (43 MHz) when using the PA or OPSY pulse sequence to monitor pH_2 addition to Vaska's complex (0.43 mM). (b) Comparison between the first usable spectrum (black) and final spectrum (red) when using the PA pulse sequence.

SI3: Simulation Development

The simulation is based on Equation S1 and accounts for consumption of the starting material (at a rate of k_{obs}) and the decay of any pre-existing hyperpolarised species (according to relaxation rate R_1).

$$\frac{d[2^*]}{dt} = k_{obs}[\mathbf{1}] - R_1[\mathbf{2}^*] \qquad [S1]$$

The simulation monitors the reaction in steps by calculating the concentrations of three species of interest: the starting material ([**1**]), the hyperpolarised product ([**2***]) and the relaxed product ([**2**]). The user is responsible for inputting the gap between each simulation step (Δt) and between each spectral acquisition (t), the starting material concentration, and the rate constants (k_{obs} and R_1) for the system of interest. At the start of the simulation, [**2***] and [**2**] are set to zero while [**1**] is set to the user input concentration.

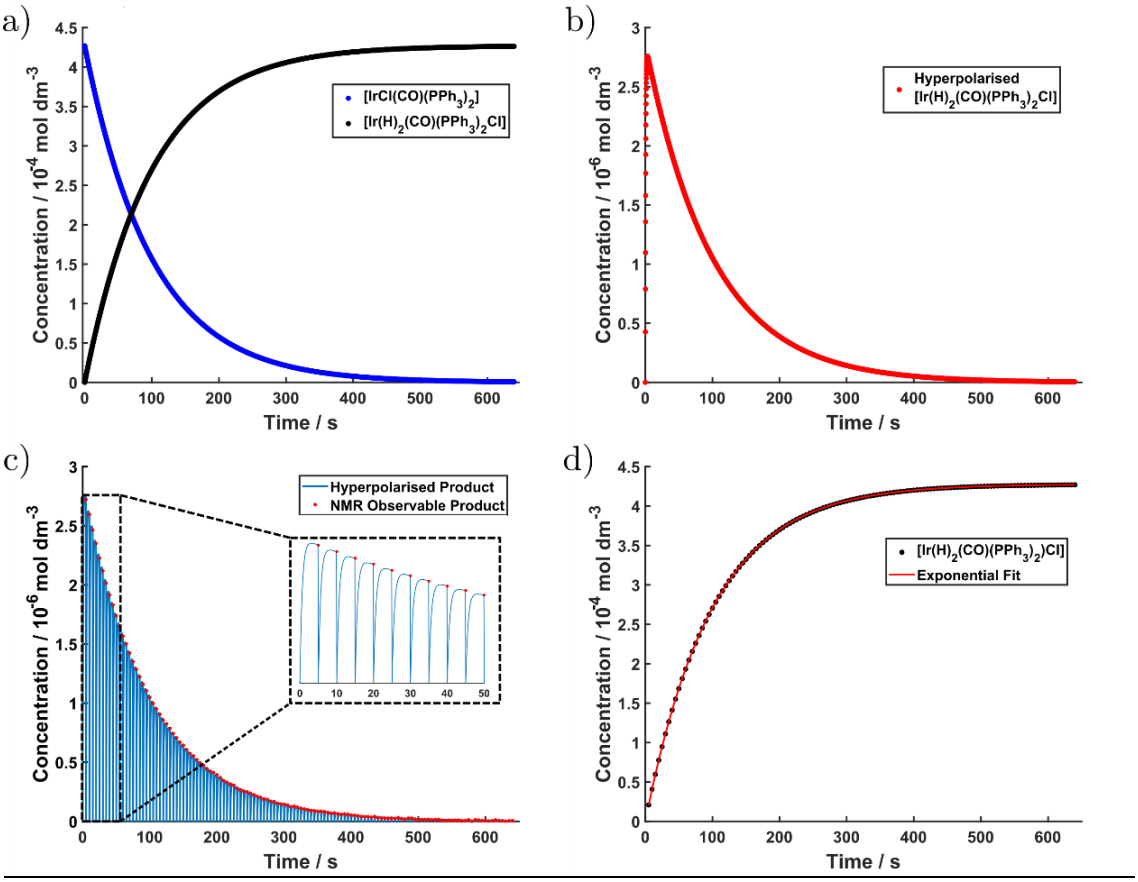

Figure S5 Simulated kinetic plots for monitoring the addition of pH_2 to *trans*-[IrCl(CO)(PPh_3)$_2$] including (a) the rates of reactant consumption and product formation, (b) formation and decay of undetected product, (c) formation and decay of sampled hyperpolarised signal and (d) the overall observed product formation curve fitted to an exponential recovery function.

For each Δt step, the previous concentration of **1** is depleted through application of k_{obs} while the concentration of **2** increases by the same amount (Figure S5a). [**2***] is calculated by applying R_1 to any leftover [**2***] from the previous time step and adding to this to the increase in [**2**]. A plot of [**2***] over time is representative of the growth and decay of the hyperpolarised signal in the absence of any spectra being recorded (Figure S5b).

To account for the collection of spectra at set time intervals, whenever the simulation reaches the time interval at which a spectrum would be taken, the concentration of **2*** is reset to 0 to model the destruction of the NMR signal upon observation. The effect of continually recording NMR spectra on the reaction profile observed is shown in Figure S5c. Finally, the observed NMR signal for each spectral acquisition can be processed identically to the experimental data and fitted to an exponential recovery function (Figure S5d). Comparison of the observed k_{obs} to the original k_{obs} input by the user indicates if the reaction monitoring method is having a notable impact on the quality of data being collected.

To account for the presence of leftover signal, a modification was made to the above simulation. Rather than resetting [**2***] to 0 upon acquisition, the concentration at that instant is multiplied by a leftover factor (determined by the user). This factor can take any value between 0 and 1, with 0 being the destruction of all hyperpolarised product and 1 meaning all signal is carried over into the next acquisition window.

The simulation was initially applied to a system similar to Vaska's complex with a k_{obs} of 0.01 s^{-1}. The simulation used 0.01 s increments, with a maximum time of 640 s and spectral acquisition occurring at intervals of either t = 5, 2.5 or 1.25 seconds. For each set of parameters, R_1 values of 15 s^{-1}, 1.5 s^{-1}, 0.15 s^{-1} and 0.015 s^{-1} were examined. Tables S2 and S3 summarise the calculated rate constant and maximum values of [**2***] for each set of parameters when using a leftover magnetisation term of 0 or 0.5 respectively.

Table S2 Summary of the k_{obs} and maximum observed [2*] values calculated via simulation for a system with an input k_{obs} of 0.01 s^{-1} and a leftover term of 0.

	t = 5.00 s		t = 2.50 s		t = 1.25 s	
R_1 / s^{-1}	**k_{obs} / s^{-1}**	**Max [2*] / mM**	**k_{obs} / s^{-1}**	**Max [2*] / mM**	**k_{obs} / s^{-1}**	**Max [2*] / mM**
15	0.00998	0.00027	0.01000	0.00028	0.01001	0.00028
1.5	0.01000	0.0027	0.01000	0.0027	0.01000	0.0024
0.15	0.01000	0.015	0.01000	0.0088	0.01000	0.0048
0.015	0.01000	0.020	0.01000	0.010	0.01000	0.0053

Table S3 Summary of the k_{obs} and maximum observed [2*] values calculated via simulation for a system with an input k_{obs} of 0.01 s^{-1} and a leftover term of 0.5.

	t = 5.00 s		t = 2.50 s		t = 1.25 s	
R_1 / s^{-1}	**k_{obs} / s^{-1}**	**Max [2*] / mM**	**k_{obs} / s^{-1}**	**Max [2*] / mM**	**k_{obs} / s^{-1}**	**Max [2*] / mM**
15	0.01000	0.00027	0.01002	0.00028	0.00999	0.00028
1.5	0.01000	0.0027	0.01000	0.0027	0.01000	0.0025
0.15	0.00999	0.017	0.00999	0.012	0.01000	0.0078
0.015	0.00991	0.032	0.00997	0.018	0.00999	0.0097

The simulation was also applied to a system reacting on the second timescale with a k_{obs} of 0.1 s^{-1}. The simulation used 0.01 s increments, with a maximum time of 80 s and spectral acquisition occurring at intervals of either t = 5, 2.5 or 1.25 seconds. For each set of parameters, R_1 values of 15 s^{-1}, 1.5 s^{-1}, 0.15 s^{-1} and 0.015 s^{-1} were examined. Tables S4 summarise the calculated rate constant and maximum values of [**2***] for each set of parameters when using a leftover magnetisation term of 0.5.

Table S4 Summary of the k_{obs} and maximum observed [2*] values calculated via simulation for a system with an input k_{obs} of 0.1 s^{-1} and a leftover term of 0.5.

	t = 5.00 s		t = 2.50 s		t = 1.25 s	
R_1 / s^{-1}	**k_{obs} / s^{-1}**	**Max [2*] / mM**	**k_{obs} / s^{-1}**	**Max [2*] / mM**	**k_{obs} / s^{-1}**	**Max [2*] / mM**
15	0.099	0.0017	0.100	0.0022	0.100	0.0025
1.5	0.100	0.018	0.100	0.023	0.100	0.022
0.15	0.094	0.11	0.095	0.088	0.097	0.060
0.015	0.076	0.17	0.088	0.12	0.095	0.072

SI4: %pH_2 Enrichment Study

Raw data for the triplicate measurements recorded during the %pH_2 enrichment study are given below in Table S5. The *para*hydrogen generator temperatures are taken from a previous study performed by Richardson *et al*.[1]

Table S5 Calculated k_2 rate constants and initial spectral SNR values for the oxidative addition of pH_2 to Vaska's complex upon varying the %pH_2 enrichment level within the sample.

%pH_2	T / K	SNR	k_2 / dm^3 mol^{-1} s^{-1}			
			1	2	3	Avg
99.04	28.0	65	0.874	0.918	0.911	0.901 ± 0.014
91.34	40.0	47	0.930	0.920	0.930	0.926 ± 0.003
80.13	49.0	44	0.893	0.925	0.922	0.88 ± 0.02
69.77	57.5	32	0.949	0.925	0.922	0.932 ± 0.008
59.78	67.0	28	1.073	0.982	0.947	1.00 ± 0.04

SI5: Tribenzylphosphine Derivative Characterisation

Low-field NMR reaction monitoring was performed to obtain kinetic information about the oxidative addition of pH_2 to trans-[IrCl(CO)(PBn_3)$_2$]. Two samples of trans-[IrCl(CO)(PBn_3)$_2$] (0.2 mg, 0.39 mM) in C_6D_6 (0.6 mL) were prepared, degassed and reacted with pH_2 (4 bar). Figure S6a shows an example ^{1}H spectrum recorded during the reaction monitoring experiment and Figure S6b shows the product formation curve for [Ir(H)$_2$Cl(CO)(PBn_3)$_2$] compared to that recorded for [Ir(H)$_2$Cl(CO)(PPh_3)$_2$]. From these reaction monitoring experiments, a k_2 of (0.83 ± 0.03) dm^3 mol^{-1} s^{-1} was obtained for the formation of [Ir(H)$_2$Cl(CO)(PBn_3)$_2$], which is slower than that observed for Vaska's complex.

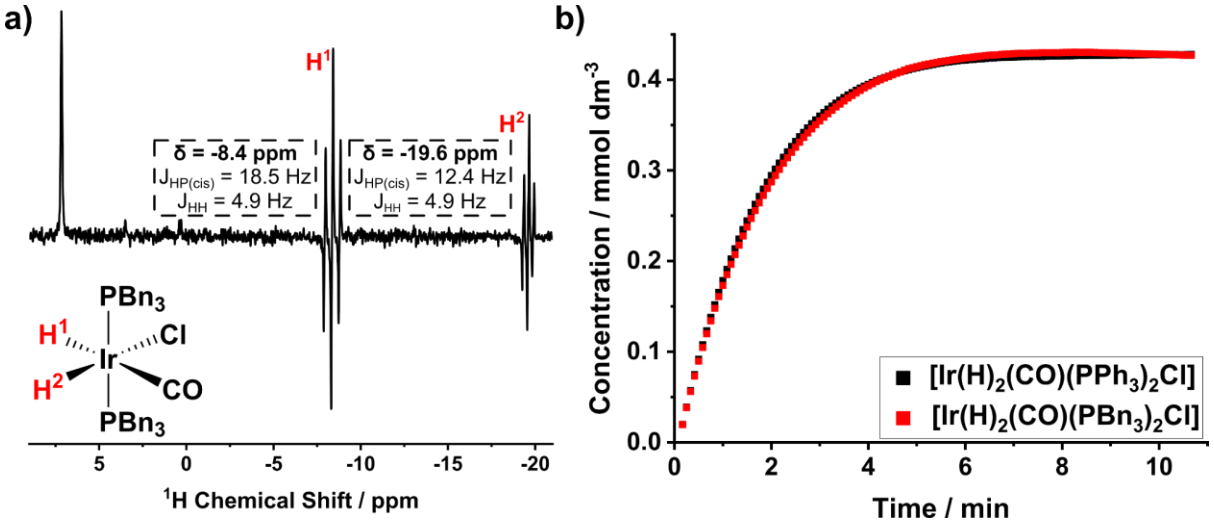

Figure 6 (a) Hyperpolarised single-scan ^{1}H spectrum and (b) a product formation curve for the reaction between pH_2 and trans-[IrCl(CO)(PBn_3)$_2$] (0.39 mM) in C_6D_6. A comparative reaction coordinate for trans-[IrCl(CO)(PPh_3)$_2$] is overlaid onto (b).

To compare the thermodynamic properties for each complex, the Eyring equation was used.[2] Reaction monitoring data was collected at high-field (9.4 T) across the temperature range of 283 – 303 K (Figure S7). Fitting of each dataset allowed for the activation enthalpy ($\Delta H^{\ddagger}$) and activation entropy ($\Delta S^{\ddagger}$) of each complex to be calculated. Using these parameters, the Gibbs free energy of

activation ($\Delta G^{\ddagger}$) at 301.5 K (the sample temperature in the benchtop NMR spectrometer) were then obtained. All values are collated within Table S7.

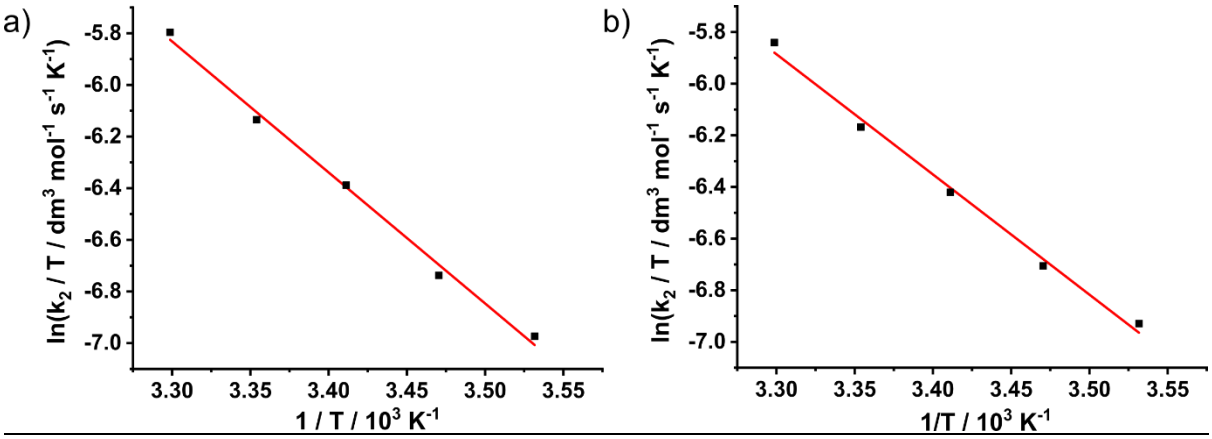

Figure S7 Eyring plots for (a) *trans*-[IrCl(CO)(PPh_3)$_2$] (0.43 mM) and (b) *trans*-[IrCl(CO)(PBn_3)$_2$] (0.39 mM) for the addition of pH$_2$ between 283 and 303 K.

Table S7 Activation energy parameters for the addition of pH$_2$ to *trans*-[IrCl(CO)(PPh_3)$_2$] (0.43 mM) and *trans*-[IrCl(CO)(PBn_3)$_2$]

Complex	$\Delta H^{\ddagger}$ / kJ mol^{-1}	$\Delta S^{\ddagger}$ / J K^{-1} mol^{-1}	$\Delta G^{\ddagger}$ (T = 301.5 K) / kJ mol^{-1}
***trans*-[IrCl(CO)(PPh_3)$_2$]**	(42 ± 2)	(-107 ± 7)	(74 ± 3)
***trans*-[IrCl(CO)(PBn_3)$_2$]**	(39 ± 2)	(-119 ± 9)	(75 ± 3)

SI6: Mixture Study Hydride Characterisation

Prior to reaction monitoring, a mixture of Vaska's complex (0.43 mM) and PBn_3 (2 eq.) was prepared, reacted with pH$_2$ and a 64 scan ^{1}H spectrum was obtained (Figure S8) in order to determine chemical shift and J coupling constant values for each species within the mixture (summarised in Table S8). This experiment was repeated using high-field NMR to reduce spectral overlap and confirm the J coupling constant values (Figure S9).

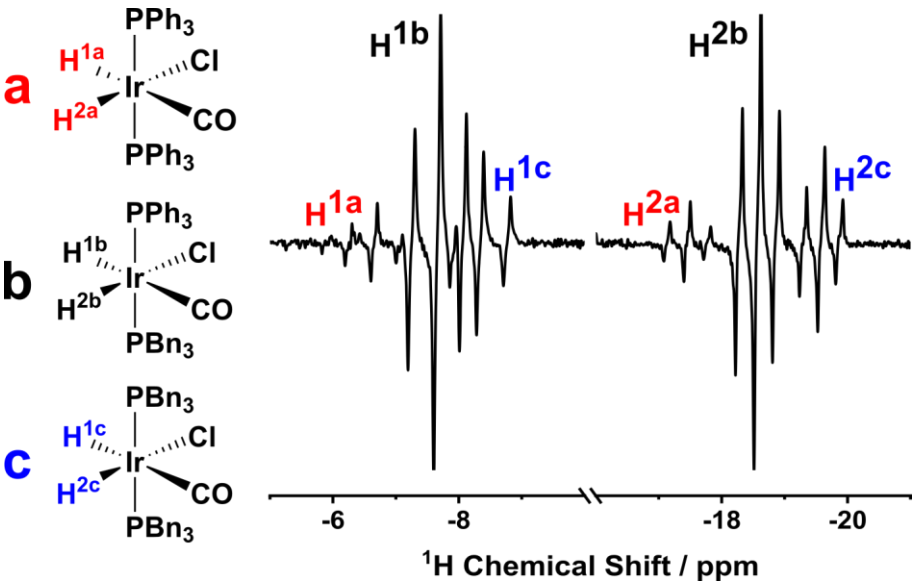

Figure S8 ^{1}H NMR spectrum of a mixture of Vaska's complex (0.43 mM) and PBn_3 (2 eq.) after pH_2 addition showing the distribution of hyperpolarised products. Recorded at 1.0 T (43 MHz) with 64 scans and an inter-scan delay of 100 ms.

Table S8 Chemical shift and J coupling constant values for $[Ir(H)_2(CO)(PPh_3)_2]$ (a), $[Ir(H)_2(CO)(PPh_3)(PBn_3)]$ (b) and $[Ir(H)_2(CO)(PBn_3)_2]$ (c) obtained from low-field NMR.

	H^1			H^2		
Complex	**δ / ppm**	**J_{HH} / Hz**	**J_{HP} / Hz**	**δ / ppm**	**J_{HH} / Hz**	**J_{HP} / Hz**
a	-6.69	4.6	17.6	-17.49	4.8	14.1
b	-7.67	4.8	17.7	-18.59	4.8	12.7
c	-8.37	4.9	18.5	-19.61	4.9	12.4

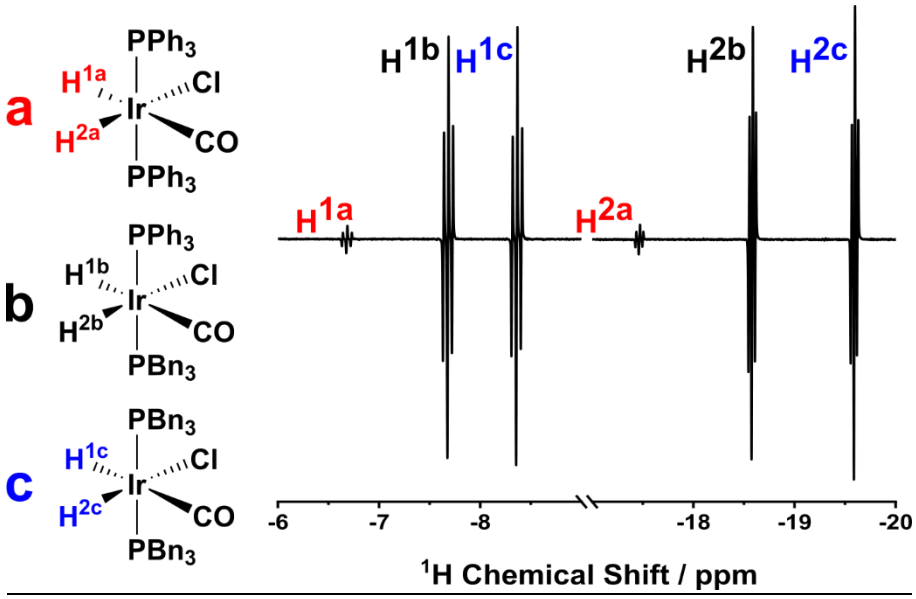

Figure S9 ^{1}H NMR spectrum of a mixture of Vaska's complex (0.43 mM) and PBn_3 (2 eq.) after pH_2 addition showing the distribution of hyperpolarised products. Recorded at 9.4 T (400 MHz) with 64 scans.

SI7: Kinetic Model for H_2 Addition to the Equilibrium Mixture

In order to model the observed rate of formation of the three hydrogenation products (**2**, **4** and **6** in Figure 7) in the presence of a dynamic equilibrium between the three starting complexes **1**, **3** and **5** (Figure 6), the following differential model (Equation S2) was implemented. k_{12}, k_{34} and k_{56} are the rates of H_2 addition to **1**, **3**, and **5**, that form **2**, **4** and **6**, respectively, while K_1 and K_2 are the associated rates of dynamic equilibrium, as defined in Figure 6.

$$
\begin{aligned}
[\mathbf{1}]_{t+\Delta t} &= [\mathbf{1}]_t - k_{12}[\mathbf{1}]_t[\mathrm{H_2}]_t\Delta t - K_1[\mathbf{1}]_t[\mathbf{5}]_t\Delta t + K_2[\mathbf{3}]_t^{\,2}\Delta t \\
[\mathbf{3}]_{t+\Delta t} &= [\mathbf{3}]_t - k_{34}[\mathbf{3}]_t[\mathrm{H_2}]_t\Delta t + 2K_1[\mathbf{1}]_t[\mathbf{5}]_t\Delta t - 2K_2[\mathbf{3}]_t^{\,2}\Delta t \\
[\mathbf{5}]_{t+\Delta t} &= [\mathbf{5}]_t - k_{56}[\mathbf{5}]_t[\mathrm{H_2}]_t\Delta t - K_1[\mathbf{1}]_t[\mathbf{5}]_t\Delta t + K_2[\mathbf{3}]_t^{\,2}\Delta t \\
[\mathrm{H_2}]_{t+\Delta t} &= -k_{12}[\mathbf{1}]_t[\mathrm{H_2}]_t\Delta t - k_{34}[\mathbf{3}]_t[\mathrm{H_2}]_t\Delta t - k_{56}[\mathbf{5}]_t[\mathrm{H_2}]_t\Delta t \\
\Delta[\mathbf{2}]_{t\to t+\Delta t} &= k_{12}[\mathbf{1}]_t[\mathrm{H_2}]_t\Delta t \\
\Delta[\mathbf{4}]_{t\to t+\Delta t} &= k_{34}[\mathbf{3}]_t[\mathrm{H_2}]_t\Delta t \\
\Delta[\mathbf{6}]_{t\to t+\Delta t} &= k_{56}[\mathbf{5}]_t[\mathrm{H_2}]_t\Delta t
\end{aligned}
\qquad \text{[S2]}
$$

In order to evaluate the model, the rates of H_2 addition to **1** and **5** were fixed to their measured values of k_{12} = 0.89 $s^{-1}M^{-1}$ and k_{56} = 0.83 $s^{-1}M^{-1}$, while the unknown rates, k_{34}, K_1 and K_2 were allowed to vary; this reduces the number of unknowns. The numerical simulation was incremented in steps of Δt = 0.01 s such that Δ[**2**], Δ[**4**], and Δ[**6**] accumulate over the observation window ΔT = 5 s. The initial concentrations $[\mathbf{1}]_0$, $[\mathbf{3}]_0$ and $[\mathbf{5}]_0$ were calculated according to Equation S3, where the total iridium concentration was set to $[\mathrm{Ir}]_{total}$ = 8.54 x 10^{-4} M, determined by the total amount of [**1**] and [**5**] added to the sample. A_0 and B_0, the relative proportions of **1** and **5** at t = 0, were allowed to vary with the initial concentration of **3** set to maintain mass balance, i.e. a fixed value of $[\mathrm{Ir}]_{total}$.

$$
\begin{aligned}
[\mathbf{1}]_0 &= A_0[\mathrm{Ir}]_{total} \\
[\mathbf{5}]_0 &= B_0[\mathrm{Ir}]_{total} \\
[\mathbf{3}]_0 &= (1 - A_0 - B_0)[\mathrm{Ir}]_{total}
\end{aligned}
\qquad \text{[S3]}
$$

The concentration of H_2 was calculated at a pressure of 4 bar to be $[\mathrm{H_2}]_0$ = 0.0118 M, as described in the main text.

In order to compare the simulated concentrations to the experimental data, the hyperpolarised integrals acquired as a function of time in N steps of duration ΔT, $I^{2*}(n\Delta T)$, $I^{2*}(n\Delta T)$, and $I^{2*}(n\Delta T)$, were normalised to the relative concentrations in the final mixture according to Equation [S4]. The final relative concentrations were determined from the relative hydride integrals in a 400 MHz NMR spectrum of the final reaction mixture. This gave values of A_{final} = 0.2, B_{final} = 0.16 and C_{final} = 0.64. Moderate variations to these final proportions were found to have no significant impact on the value determined for the unknown rate, k_{34}.

$$[\mathbf{2}]_{exp}(n\Delta T) = A_{final}[Ir]_{total}\frac{I_{2^*}(n\Delta T)}{\sum_{m=1}^{N} I_{2^*}(m\Delta T)}$$

$$[\mathbf{4}]_{exp}(n\Delta T) = C_{final}[Ir]_{total}\frac{I_{4^*}(n\Delta T)}{\sum_{m=1}^{N} I_{4^*}(m\Delta T)} \qquad [S4]$$

$$[\mathbf{6}]_{exp}(n\Delta T) = B_{final}[Ir]_{total}\frac{I_{6^*}(n\Delta T)}{\sum_{m=1}^{N} I_{6^*}(m\Delta T)}$$

This numerical simulation was implemented in Matlab and optimised using the *fminsearch* algorithm to minimise the sum-of-squared-differences between the simulated and experimental data, according to Equation [S5].

$$x = \sum_{n=1}^{N}\left[\begin{array}{l}\left(\Delta[\mathbf{2}]_{(n-1)\Delta T\to n\Delta T} - [\mathbf{2}]_{\exp}\left(n\Delta T\right)\right)^2 + \left(\Delta[\mathbf{4}]_{(n-1)\Delta T\to n\Delta T} - [\mathbf{4}]_{\exp}\left(n\Delta T\right)\right)^2 \\ + \left(\Delta[\mathbf{6}]_{(n-1)\Delta T\to n\Delta T} - [\mathbf{6}]_{\exp}\left(n\Delta T\right)\right)^2\end{array}\right] \qquad [S5]$$

Table S9 Optimised parameters obtained for fits of three independent samples to the model.

Parameter	Sample 1	Sample 2	Sample 3	Average
K_1 / s^{-1} M^{-2}	43	47	60	50 ± 5
K_2 / s^{-1} M^{-2}	5.3	6.2	11.5	7.6 ± 1.9
k_{56} / s^{-1} M^{-1}	1.02	1.18	1.57	1.26 ± 0.16
A_0	0.20	0.21	0.24	0.221 ± 0.013
B_0	0.17	0.18	0.21	0.187 ± 0.011

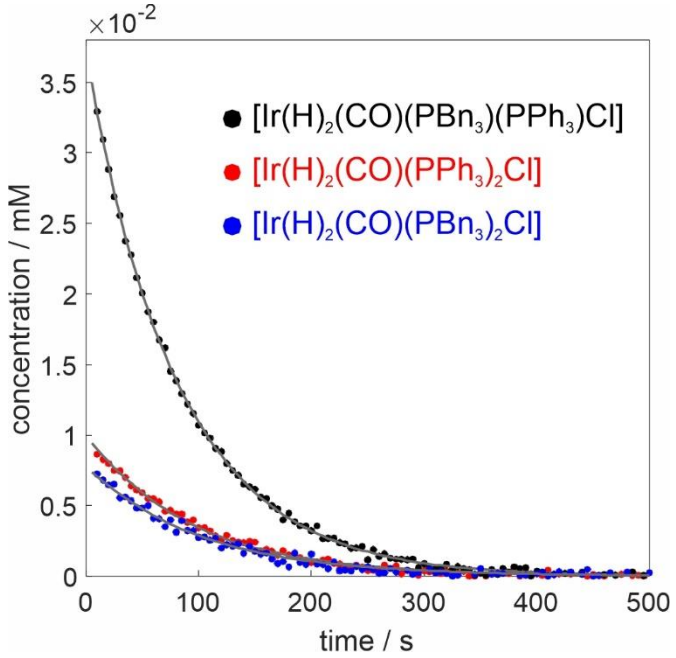

Figure S10 Fit of the kinetic model in Equation S2 (gray lines) to the experimental integrals (black, red and blue circles for 4*, 2* and 6*, respectively) for Sample 2 using the parameters in Table S8 and Equation S4 to scale the integrals to the distribution in the final mixture following reaction completion.

The model proves to yield a good fit for three independent samples with rates k_{12} and k_{56} fixed to their measured values (see example fit in Figure S10). However, as indicated by the fitting parameters in Table S9, a larger variation in the unknown rate, k_{34}, was observed across the three repeat samples than was found for the single component experiments. Notably, a significantly faster rate was observed for Sample 3 in particular. We identify this as originating from differences in sample handling. For example, differential solvent loss during the degassing step would lead to different increases in concentration that would impact directly on the underlying equilibrium changes and the effective rate of H_2 addition for the biomolecular step. The need for k_{34} to be larger than k_{12} and k_{56} is not however in doubt when these data are visually inspected.

References

1) P. M. Richardson, R. O. John, A. J. Parrott, P. J. Rayner, W. Iali, A. Nordon, M. E. Halse and S. B. Duckett, *Phys. Chem. Chem. Phys.*, 2018, **20**, 26362-26371.
2) H. Eyring, *J. Chem. Phys.*, 1935, **3**, 107.